Research Article | Vol. 26, No. 6 | 19 Mar 2018 | OPTICS EXPRESS 7771
Optics EXPRESS

Temperature effects on tunable cw Alexandrite lasers under diode end-pumping

WILLIAM R. KERRIDGE-JOHNS* AND MICHAEL J. DAMZEN

Photonics Group, Department of Physics, Imperial College London, London SW7 2AZ, UK
*wrk10@ic.ac.uk

Abstract: Diode pumped Alexandrite is a promising route to high power, efficient and inexpensive lasers with a broad (701 nm to 858 nm) gain bandwidth; however, there are challenges with its complex laser dynamics. We present an analytical model applied to experimental red diode end-pumped Alexandrite lasers, which enabled a record 54 % slope efficiency with an output power of 1.2 W. A record lowest lasing wavelength (714 nm) and record tuning range (104 nm) was obtained by optimising the crystal temperature between 8 °C and 105 °C in the vibronic mode. The properties of Alexandrite and the analytical model were examined to understand and give general rules in optimising Alexandrite lasers, along with their fundamental efficiency limits. It was found that the lowest threshold laser wavelength was not necessarily the most efficient, and that higher and lower temperatures were optimal for longer and shorter laser wavelengths, respectively. The pump excited to ground state absorption ratio was measured to decrease from 0.8 to 0.7 by changing the crystal temperature from 10 °C to 90 °C.

Published by The Optical Society under the terms of the Creative Commons Attribution 4.0 License. Further distribution of this work must maintain attribution to the author(s) and the published article's title, journal citation, and DOI.

OCIS codes: (140.3480) Lasers, diode-pumped; (140.5680) Rare earth and transition metal solid-state lasers; (140.6810) Thermal effects.

References and links

1. J. Walling, O. Peterson, H. Jenssen, R. Morris, and E. O'Dell, "Tunable Alexandrite lasers," IEEE J. Quantum Electron. **16**, 1302–1315 (1980).
2. J. W. Kuper, T. Chin, and H. E. Aschoff, "Extended Tuning Range of Alexandrite at Elevated Temperatures," in *Advanced Solid State Lasers,* Vol. 6 of OSA Proceedings Series (Optical Society of America, 1990), paper CL3.
3. A. Teppitaksak, A. Minassian, G. Thomas, and M. Damzen, "High efficiency >26 w diode end-pumped alexandrite laser," Opt. Express **22**, 16386–16392 (2014).
4. E. Arbabzadah and M. Damzen, "Fibre-coupled red diode-pumped alexandrite TEM00 laser with single and double-pass end-pumping," Laser Phys. Lett. **13**, 065002 (2016).
5. J. Walling, D. Heller, H. Samelson, D. Harter, J. Pete, and R. Morris, "Tunable Alexandrite lasers: Development and performance," IEEE J. Quantum Electron. **21**, 1568–1581 (1985).
6. M. Lando, Y. Shimony, R. M. Benmair, D. Abramovich, V. Krupkin, and A. Yogev, "Visible solar-pumped lasers," Opt. Mater. **13**, 111 – 115 (1999).
7. P. Pichon, A. Barbet, J.-P. Blanchot, F. Druon, F. Balembois, and P. Georges, "Led-pumped alexandrite laser oscillator and amplifier," Opt. Lett. **42**, 4191–4194 (2017).
8. S. T. Lai and M. L. Shand, "High efficiency cw laser-pumped tunable alexandrite laser," J. Appl. Phys. **54**, 5642–5644 (1983).
9. J. Kuper and D. Brown, "High efficiency cw green-pumped alexandrite lasers," Proc. SPIE **6100**, 61000T (2006).
10. M. J. Damzen, G. M. Thomas, and A. Minassian, "Diode-side-pumped alexandrite slab lasers," Opt. Express **25**, 11622–11636 (2017).
11. E. Beyatli, I. Baali, B. Sumpf, G. Erbert, A. Leitenstorfer, A. Sennaroglu, and U. Demirbas, "Tapered diode-pumped continuous-wave Alexandrite laser," J. Opt. Soc. Am. B **30**, 3184–3192 (2013).
12. I. Yorulmaz, E. Beyatli, A. Kurt, A. Sennaroglu, and U. Demirbas, "Efficient and low-threshold Alexandrite laser pumped by a single-mode diode," Opt. Mater. Express **4**, 776–789 (2014).
13. M. Shand, J. Walling, and H. Jenssen, "Ground state absorption in the lasing wavelength region of Alexandrite: Theory and experiment," IEEE J. Quantum Electron. **18**, 167–169 (1982).
14. M. Shand, J. Walling, and R. Morris, "Excited-state absorption in the pump region of Alexandrite," J. Appl. Phys. **52**, 953–955 (1981).
15. M. Shand and J. Walling, "Excited-state absorption in the lasing wavelength region of Alexandrite," IEEE J. Quantum Electron. **18**, 1152–1155 (1982).

#319433 https://doi.org/10.1364/OE.26.007771
Journal © 2018 Received 31 Jan 2018; revised 6 Mar 2018; accepted 7 Mar 2018; published 16 Mar 2018

Optics EXPRESS

16. M. Strotkamp, U. Witte, A. Munk, A. Hartung, S. Gausmann, S. Hengesbach, M. Traub, H.-D. Hoffmann, J. Hoeffner, and B. Jungbluth, "Broadly tunable, diode pumped alexandrite laser," in *Advanced Solid-State Lasers Congress,* OSA Technical Digest (Optical Society of America, 2013), paper ATu3A.42.
17. W. R. Kerridge-Johns and M. J. Damzen, "Analytical model of tunable alexandrite lasing under diode end-pumping with experimental comparison," J. Opt. Soc. Am. B **33**, 2525–2534 (2016).
18. Z. Zhang, K. Grattan, and A. Palmer, "Thermal characteristics of Alexandrite fluorescence decay at high temperatures, induced by a visible laser diode emission," J. Appl. Phys. **73**, 3493–3498 (1993).
19. D. McCumber, "Theory of phonon-terminated optical masers," Phys. Rev. **134**, A299–A306 (1964).
20. W. R. Kerridge-Johns and M. J. Damzen, "Analysis of pump excited state absorption and its impact on laser efficiency," Laser Phys. Lett. **12**, 125002 (2015).
21. M. Fibrich, J. Šulc, D. Vyhlídal, H. Jelínková, and M. Čech, "Alexandrite spectroscopic and laser characteristic investigation within a 78-400k temperature range," Laser Phys. **27**, 115801 (2017).
22. R. Scheps, J. F. Myers, T. R. Glesne, and H. B. Serreze, "Monochromatic end-pumped operation of an alexandrite laser," Optics Communications **97**, 363 – 366 (1993).
23. M. Shand and H. Jenssen, "Temperature dependence of the excited-state absorption of Alexandrite," IEEE J. Quantum Electron. **19**, 480–484 (1983).

1. Introduction

Lasers with tunable output wavelengths are beneficial in many applications, for example in remote sensing or scientific studies. Alexandrite, Cr^{3+}:$BeAl_2O_4$, is an attractive gain medium for these applications due to its broadly tunable vibronic emission between 701 nm to 858 nm [1, 2], excellent thermo-mechanical properties [1] and efficiency [3, 4].

Many pumping schemes have been applied to Alexandrite. Historically flashlamp pumping has been the most prolific [5]; however, solar [6], LED [7], Krypton ion [8], frequency doubled Neodymium [9], and red laser diode side [10] and end [3] pumping have been demonstrated. Of these techniques, diode-end pumping has been shown to be a route to efficient and high beam quality operation.

A diode end-pumped slope efficiency in Alexandrite as high as 44 % with a TEM_{00} mode has been achieved [4]. High power red diodes have achieved a laser power output of 26 W in multimode operation [3]. Wavelength tuning of diode pumped systems has been attempted, with the shortest reported wavelength of 724 nm [11], longest at 823 nm [12], and greatest total wavelength tuning range of 92 nm in a single system [11].

Alexandrite has a range of competing effects across its gain spectrum. In addition to the wavelength dependent emission cross section, these include ground state absorption (GSA) at laser wavelengths [13] and excited state absorption (ESA) at both pump [14] and laser [15] wavelengths. The complex spectral interplay of these lead to differing conditions for optimal laser performance. A key parameter and further complexity is the temperature of the gain medium, which has been shown to be important in optimising power output and crucial to accessing the full tuning range available in Alexandrite [2]. Previous works have shown by experiment the effect of temperature on Alexandrite performance [12, 16], but were limited in scope to the specific systems investigated and the conclusions drawn are not necessarily applicable to Alexandrite lasers in general.

The aim of this work is to elucidate, quantify and predict the effect of temperature on laser performance in diode-pumped Alexandrite, yielding rules useful in general to optimising specific Alexandrite lasers. This involves understanding the temperature impact on these wavelength dependent processes, in addition to the upper-state lifetime, and provides practical advice for cw laser optimisation.

We present results from diode end-pumped laser cavities both with and without wavelength selective elements, and show the performance that can be achieved along with the impact of temperature on the laser operation. An end-pumped quasi three level theory is described and shown to be suitable for prediction of laser performance and a useful tool for Alexandrite laser design. The effect of temperature on the pump ESA cross section at 637 nm in Alexandrite was determined for the first time experimentally.

Optics EXPRESS

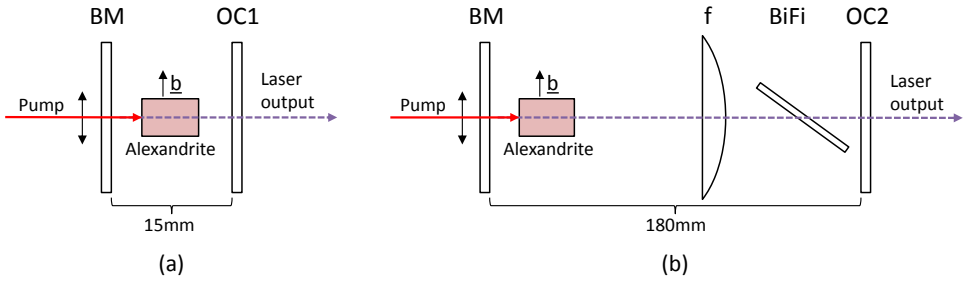


Fig. 1. The two cavity configurations investigated: (a) compact and (b) extended tunable. The pump was polarised parallel to the b-axis of the Alexandrite. The laser wavelength of the extended cavity could be tuned with the birefringent filter (BiFi).

2. Experimental systems

The Alexandrite lasers investigated had the two laser cavity configurations as shown in Fig. 1. The back mirror (BM) was dichroic with high transmission for the pump and high reflectance at laser wavelengths and was common to both cavities. The output coupler (OC) had two positions of OC1 and OC2. A 'compact' cavity, Fig. 1(a), was formed in position OC1 with cavity length 15 mm. An 'extended' cavity, Fig. 1(b), with position OC2 was used to accommodate an intracavity birefringent filter (BiFi) for laser wavelength control. To maintain cavity stability and control the laser mode size on the crystal an $f = 10$ cm focal length lens was used in the extended cavity, which had a super-V coating centred on 760 nm with a per surface loss of 0.03 %, rising to 0.18 % 40 nm either side. The output coupler for OC1 and OC2 was the same, with a reflectance of 99.5 % at 700 nm, decreasing to 99.2 % at 820 nm. The compact cavity was additionally tested with a 95.2 % reflectance output coupler.

End-pumping of the laser was with a 5 W fibre coupled diode module with 105 µm core diameter and NA = 0.22. The pump was then polarised, giving a maximum 3.07 W incident power at 636 nm, and its polarisation aligned with the b-axis of the Alexandrite crystal with a half wave plate. It was focussed with an aspheric lens of focal length $f_p = 20$ mm, producing a focal waist diameter of 150 µm, $M^2 = 45$ and Rayleigh length 0.6 mm in air. The crystal used was a 0.22 at.% Cr-doped Alexandrite rod, which was 4 mm long with a diameter of 2 mm. It had a measured pump absorption coefficient of 7.5 cm^{-1} and absorbed 95 % of incident pump radiation. It was held in a water cooled copper mount with a TEC controlled temperature range of 8 °C to 105 °C.

2.1. Compact cavity

The laser output power versus absorbed pump power of the compact cavity, Fig. 1(a), is shown in Fig. 2. The output power was 1.22 W at 762 nm from an absorbed pump power of 2.74 W. The threshold was at 0.46 W absorbed pump power and the laser had a slope efficiency of $\eta_s = 54$ %, which is to our knowledge the highest slope efficiency diode-pumped Alexandrite laser to date. The output beam was TEM_{00} with a high beam quality of $M^2 = 1.08$. The spatial profile is shown in the inset image of Fig. 2. The measured output beam waist diameter was 180 µm at the OC, which compared to the pump beam size of 150 µm is consistent with the excellent beam mode overlap efficiency. The spectrum of the output is shown in the inset graph of Fig. 2 with the crystal oven temperature at 70 °C, the central laser wavelength was 762 nm with broad full-width half maximum (FWHM) of 5.7 nm, which is typical in Alexandrite [12]. The compact cavity design benefited from being very low loss, with an approximate round trip loss of 0.2 %, which was determined through direct loss measurements of the intra-cavity optics.

Coarse tuning of the compact cavity was achieved by altering the crystal temperature, with its

Optics EXPRESS

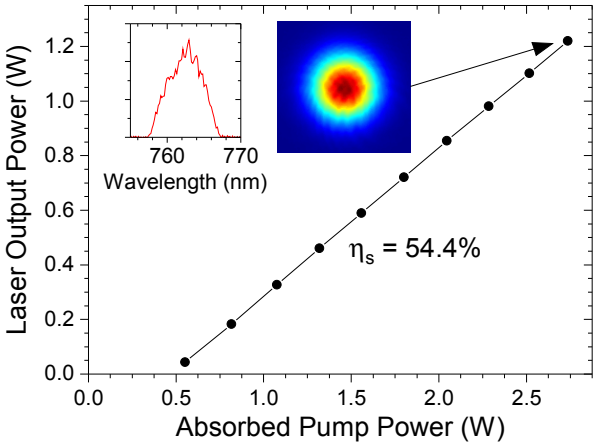


Fig. 2. The laser output power versus absorbed pump power for the compact cavity with a record slope efficiency of 54.4 %. *Inset*: Spatial mode profile at 1.22 W output power and the laser wavelength spectrum.

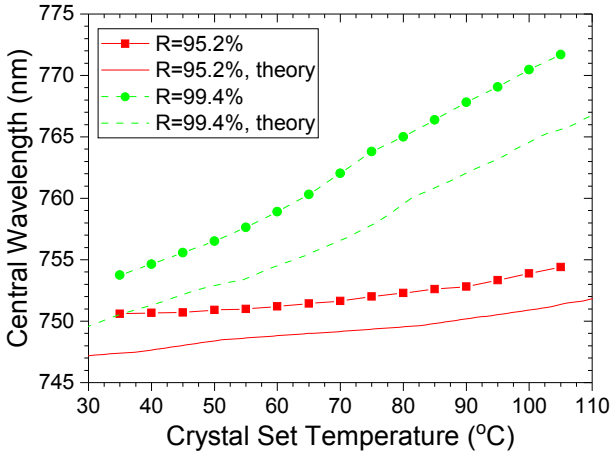


Fig. 3. The laser wavelength versus crystal temperature in the compact cavity for output coupler reflectances R. The theoretical predictions are also shown based on the model in Section 4

effect on the central laser wavelength shown in Fig. 3. The theoretical operation wavelength is also shown, calculated from a previously presented model [17] and summarised in Section 4. The wavelength that minimised the threshold at a given temperature was found, which due to gain clamping would be the oscillating laser mode. The offset between theory and experiment could be from there being a higher crystal temperature than that of the crystal oven set temperature, future studies would benefit from calibration of this offset either through probe measurements or simulation. Additionally, there were uncertainties in the properties of Alexandrite and the optical coating reflectances put into the model.

The maximum tuning range achieved solely via crystal temperature control was 18 nm centred on 763 nm with an output coupler reflectance of R = 99.4 %. However, this range reduced to 4 nm with R = 95.2 %. This shows that wavelength tuning is possible in Alexandrite via crystal temperature control when no wavelength selective elements are used, as shown in other

Optics EXPRESS

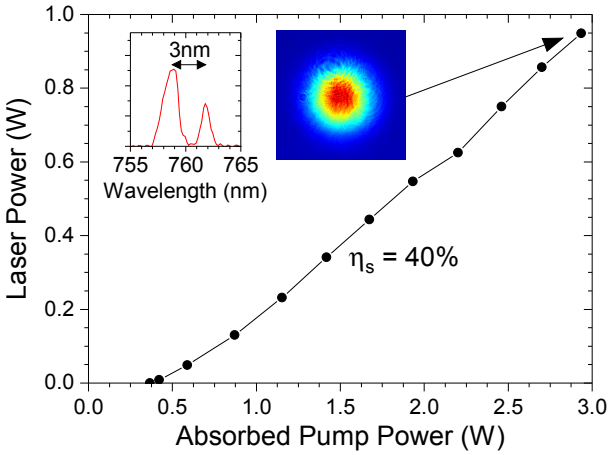


Fig. 4. The output laser power versus input pump power for the extended cavity with no birefringent plate. The Alexandrite crystal temperature was 60 °C. *Inset*: Spatial mode profile at 0.95 W output power and the laser wavelength spectrum.

studies [12], but has a small range compared to the gain bandwidth available and is limited to the central gain region. The tuning range possible solely from crystal temperature control is generally much smaller than the range possible with dedicated wavelength control methods.

2.2. *Extended wavelength tunable cavity*

The extended cavity laser, shown in Fig. 1(b), was first operated without the birefringent element. The laser output power versus pump input power is shown in Fig. 4 for a crystal temperature of 60 °C. It operated with a central wavelength of 760 nm at maximum pump power, a slope efficiency of 40 % and a TEM_{00} spatial mode profile, shown in the inset of Fig. 4. The inset graph shows the output spectrum, consisting of two peaks separated by 3 nm, this is typical of a free-running Alexandrite laser and is attributed to birefringence in the crystal [12].

The extended cavity was then operated with an intracavity 0.5 mm thick quartz plate BiFi for tuning the laser wavelength. It was aligned at the Brewster angle and had a measured reflective round trip loss of 0.01 %. The laser power versus wavelength is shown in Fig. 5(a), where the crystal temperature was optimised from between 8 °C and 105 °C to achieve the maximum laser output power at each wavelength. The laser power with wavelength at a fixed crystal temperature of 60 °C is also shown for comparison. The flat portions of the optimum temperature curve correspond to the limits of the TEC equipment for the oven temperature control. Figure 5(b) shows the typical laser frequency spectrum when using the BiFi, measured with a Fabry-Perot etalon. It consisted of multiple longitudinal modes separated by 680 MHz with a total FWHM of 2.1 GHz.

The laser was tunable from 714 nm to 818 nm, a record lowest wavelength and largest range for a vibronic emission diode pumped Alexandrite system. Key to achieving this tuning range was adapting the temperature of the Alexandrite crystal. A wider tuning range and higher output powers at both the upper and lower wavelength limits would have been possible without the 8 °C to 105 °C limit of the oven used.

The wavelength tuning was continuous up to approximately 10 nm from the extremes, at this point the laser had regions of 5 nm width where it would not lase. It is likely that the crystal birefringence was interfering with the tuning effect of the birefringent element in these areas [12].

The beam quality was lower than without the BiFi, with M^2 = 2.3 and 1.5 in the horizontal and vertical planes, respectively, but gave approximately 20 % higher output power than when

Optics EXPRESS

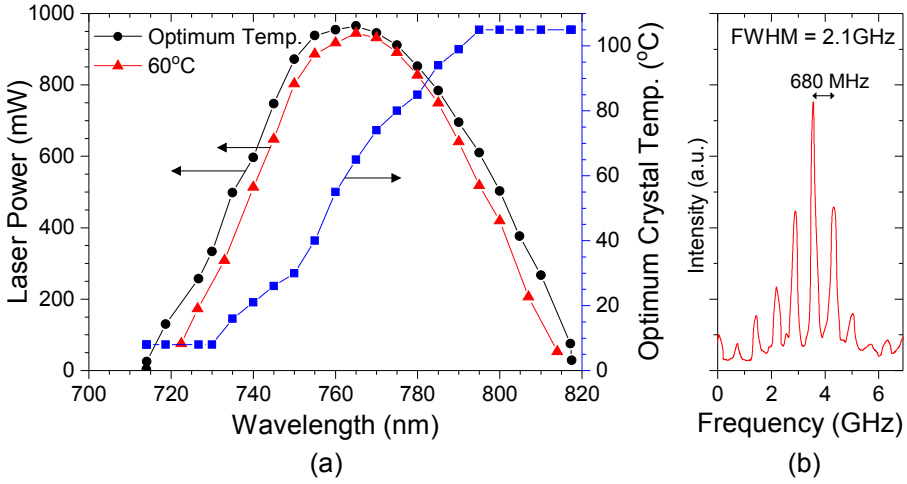


Fig. 5. (a) The laser output power versus laser wavelength at the optimum crystal temperature and at a fixed crystal temperature of 60 °C. The optimum crystal temperature is given on the right axis of the graph. (b) The typical frequency spectrum of the output, with a full-width half maximum of 2.1 GHz.

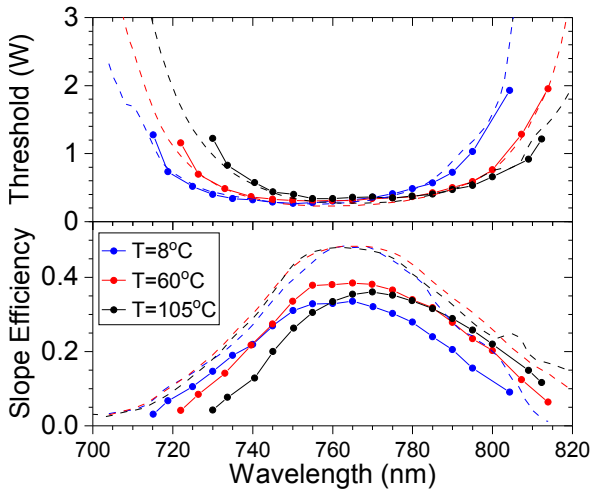


Fig. 6. The threshold (top) and slope efficiency (bottom) of the laser at 10 °C, 60 °C and 105 °C crystal temperatures (T) against laser output wavelength. Dashed curves are the results of the analytical model.

operated with an M^2 close to one.

The output laser power variation is useful in giving an overview of laser performance across the lasing spectrum, but to understand its behaviour more fundamentally the slope efficiency and threshold are useful measures. The threshold pump powers for lasing and slope efficiencies at different crystal temperatures (10 °C, 60 °C, 105 °C) across the output laser spectrum with comparison to model results are shown in Fig. 6, relative to absorbed pump power.

The underlying causes of the output power changes in Fig. 5 are apparent from Fig. 6. Towards the edges of the tuning range the thresholds increased and slope efficiencies decreased, resulting in the reduced output power. At short laser wavelengths the thresholds were reduced at lower

Optics EXPRESS

temperatures, which was opposite to the trend at longer wavelengths, where higher temperatures decreased the laser threshold.

The experimental results were a close fit to the theoretical predictions for the thresholds showing the validity of the model. The experimental tuning range was smaller than predicted by theory with 2.9 W of absorbed pump power available. This was partly from the approximate 100 nm free spectral range of the BiFi that prevented lasing with a high threshold at one tuning range extreme, where a lower threshold wavelength existed at the other. Additionally, the approximately discrete 5 nm steps at the tuning range extremes limited the tuning range by a few nanometers at each end.

The slope efficiencies had similar trends in experiment and modelling. At longer wavelengths the higher slope efficiency with increased temperature was predicted. At shorter wavelengths the trend with temperature is less well matched. The discrepancy was likely due to spatial mode matching efficiency not being included in the modelling. This would have more significantly affected shorter wavelengths, where low spatial overlap of the laser mode and lesser pumped regions would result in greater laser GSA than the plane wave model.

The optimum output power for the extended cavity was at a wavelength of 765 nm, Fig. 5. However, when operated with no BiFi control, the laser wavelength was 760 nm at 60 °C. The cause of this seeming discrepancy is that the wavelengths for the lowest threshold and highest slope efficiency were not coincident. The free running laser operated at its lowest threshold wavelength of 760 nm, the lowest threshold of the tuned laser was also at approximately 760 nm, Fig. 6. However, the optimum power output was achieved at the longer wavelength of 765 nm, closer to where the slope efficiency was highest at 770 nm.

The mismatch of lowest threshold and maximum slope efficiency is explained in Section 4, and is due to the different spectral forms of the laser emission and ESA cross section. This behaviour suggests that in general Alexandrite lasers can benefit from a wavelength selective element to optimise power output by forcing it to lase at a higher threshold, but where it also has a larger slope efficiency. The significance of this effect will increase when operating at pump powers further away from threshold.

The best laser performance was obtained from the compact cavity in terms of threshold pump power, slope efficiency and output power. The highest slope efficiencies achieved in the compact and extended cavities were 54 % and 40 %, respectively. The reduced efficiency in the extended cavity was a combination of increased losses from additional intracavity optical components and a likely poorer match between the pump and laser modes.

The experimental systems show complicated behaviour across the wavelength tuning range, particularly with regard to the crystal temperature. This is the result of a complex interplay of factors and is best explained through interrogation of a model, where parameters not readily accessible in experiments can be isolated to explain different features in the experiment.

3. Alexandrite optical properties

In order to evaluate the performance of the presented, or any other, Alexandrite laser the characteristics of the medium itself must be understood. Alexandrite can be modelled as a quasi-three level laser, with the additional effects of pump and laser ESA. A representative energy level model is shown in Fig. 7. The pump is absorbed from the ground state into a pump band with cross section σ_0. Laser gain is through stimulated emission from level 1 to 0 with cross section σ_e. Laser GSA causes reabsorption of laser photons, with cross section σ_a. There is also ESA at the pump and laser wavelengths from the upper laser level, with cross sections σ_1 and σ_{1a} respectively. Non-radiative decays occur from levels 2 and 3 to the upper laser level with lifetimes τ_{21} and τ_{31}, which are assumed to be instantaneous. Fluorescent decay occurs from level 1 to 0 with a lifetime τ_f. The cross sections described are all effective values as levels 0, 1 and 2 are in reality manifolds of states.

The cross sections can be taken from measurements in the literature, however the laser GSA

Optics EXPRESS

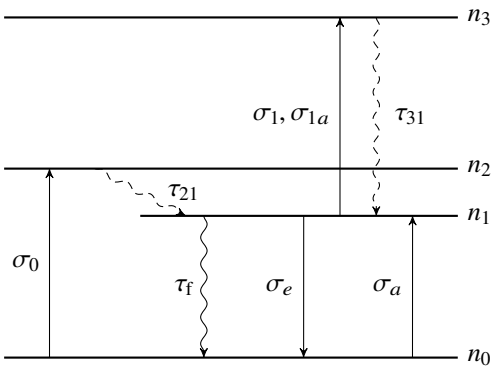


Fig. 7. Diagram of the energy level structure of a quasi-three level laser, with a fourth level providing ESA at the pump wavelength. *Parameters*: n_i are the populations of the ith levels; σ_0 and σ_1 are the pump ground and excite-state absorption cross sections, respectively; σ_a and σ_{1a} are the laser ground and excited-state absorption cross sections, respectively; σ_e is the laser emission cross section; τ_f is the laser level fluorescence lifetime; τ_{21} and τ_{31} are non-radiative lifetimes.

cross section [13] and fluorescence lifetime [18] variations as functions of temperature are well approximated from mathematical relations. The laser GSA cross section is related to the emission cross section by the extended McCumber relation [19], which causes it to exponentially increase with temperature and shortening wavelength. It is given by

$$\sigma_a(T, E) = \sigma_e(T, E)\mathrm{e}^{\frac{[E-E^*(T)]}{k_\mathrm{b}T}}, \tag{1}$$

where T is the crystal temperature, E is the laser photon energy and E^* is the effective no phonon energy ($E < E^*$).

The dependence of the transition cross sections on laser wavelength gives Alexandrite three regimes of operation as indicated in Fig. 8. Below 760 nm it is an increasingly quasi-three-level system with additional increasing laser ESA. Above 760 nm the laser GSA cross section becomes negligible, so from 760 nm to 780 nm it is approximately a 4-level laser with the ESA cross section becoming zero at 770 nm. Above 780 nm the lasing is 4-level, with an increasing influence of ESA at longer wavelengths. At 828 nm and a crystal temperature of 28 °C the laser ESA and emission cross sections are equal and no gain is possible, forming an upper wavelength limit. The boundaries between the lasing regimes are not well defined and are presented as a guide to understanding the behaviour of Alexandrite.

Another consideration in Alexandrite is the crystal temperature, which further affects the lasing regimes. The dominant cause of temperature related effects in Alexandrite is due to the upper laser level being split between two sub-levels. These have an effective separation of approximately $\triangle E = 800\,\mathrm{cm}^{-1}$ so have a thermal Boltzmann population distribution between them [1]. The upper sub-level ($^4\mathrm{T}_2$) has stronger vibronic transitions with a lifetime of $\tau_\mathrm{T} = 6.6\,\mu\mathrm{s}$. The lower sub-level ($^2\mathrm{E}$) has a lifetime of $\tau_\mathrm{E} = 1.54\,\mathrm{ms}$ and mostly acts as a storage state. The total upper state fluorescence lifetime is given by

$$\tau_\mathrm{f} = \tau_\mathrm{E}\left[\frac{1 + \mathrm{e}^{-\triangle E/k_\mathrm{b}T}}{1 + (\tau_\mathrm{E}/\tau_\mathrm{T})\mathrm{e}^{-\triangle E/k_\mathrm{b}T}}\right], \tag{2}$$

where k_b is the Boltzmann constant [1]. The effect of crystal temperature on the fluorescence lifetime and net emission cross section is shown in Fig. 9, with the product of the two parameters indicating the pump intensity required to reach laser threshold. The higher product at increasing

Optics EXPRESS

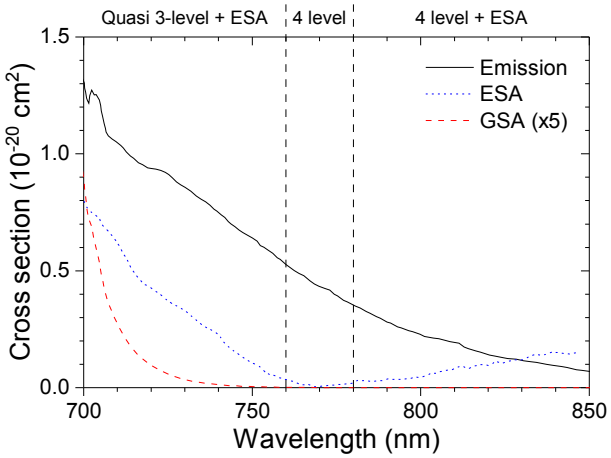


Fig. 8. The laser GSA, ESA and emission cross sections with wavelength at 28 °C. The GSA cross section has been magnified by a factor of 5. The three regimes of operation are indicated.

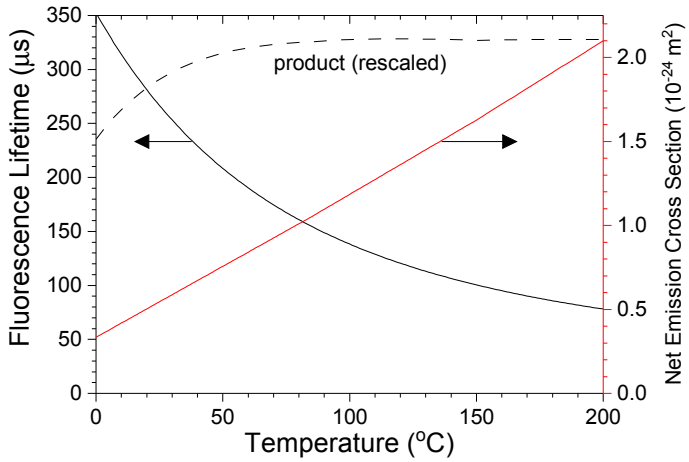


Fig. 9. The fluorescence lifetime (black), net emission cross section ($\sigma_e - \sigma_{1a}$) at 760 nm (red), and their rescaled product in arbitrary units (dashed) against crystal temperature in Alexandrite.

temperatures indicates a lower laser threshold, which demonstrates a potential benefit to higher temperatures in Alexandrite.

3.1. Pump ESA cross section

Pump excited state absorption has been previously measured in Alexandrite [14, 17] and shown to be an important factor in understanding and optimising laser performance [20]. Pump ESA can be quantified as the ratio of ESA to GSA cross sections, $\gamma = \sigma_1/\sigma_0$, with previous measurements giving $\gamma = 0.76 \pm 0.01$ at 637 nm and 20 °C. However, there are significant temperature dependences in Alexandrite, yet there has been no previous investigation on the effect of crystal temperature on the pump ESA.

To address this, the pump ESA ratio γ was measured at different crystal temperatures through the saturating transmission of an Alexandrite sample, following a previous experimental design [17].

Optics EXPRESS

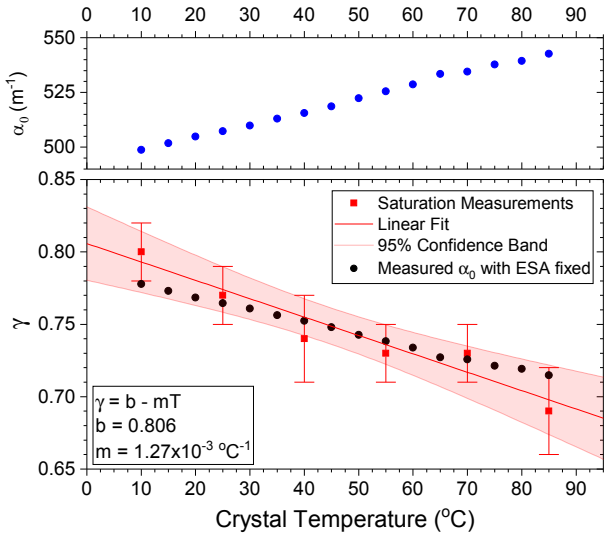


Fig. 10. *Bottom* - The pump ESA to GSA ratio γ values (red squares) against crystal temperature with a linear fit and 95 % confidence band (red area). Also shown is how γ would change assuming the ESA cross section is constant and measured GSA changes in α_0 (black points). *Top* - The GSA coefficient (α_0) against crystal temperature from small signal transmission measurements.

This method was enhanced by changing the probe beam diameter to more precisely measure the small signal transmission of the crystal. The pump ESA ratio γ measurements against crystal temperature are shown in Fig. 10 (red squares), with a linear fit calculated and 95 % confidence bands. These results show a decrease in γ when going to higher crystal temperatures, with γ approximately 0.8 at 10 °C and 0.7 at 90 °C.

The GSA coefficient is $\alpha_0 = \sigma_0 N$, where N is the active ion population density. It was measured through the small signal transmission and is shown in Fig. 10 as a function of crystal temperature, it was found to increase as has been previously reported [18, 21].

The ESA coefficient ($\alpha_1 = \sigma_1 N$) can be determined using $\gamma = \alpha_1/\alpha_0$, which from the measured γ values is $\alpha_1 = 388\,\mathrm{m}^{-1}$ at 45 °C. Assuming the pump ESA coefficient remains constant at that value, the expected γ from the measured α_0 is shown in Fig. 10 (black points). The close match between the two data sets indicates that the observed γ temperature dependence could be solely due to the temperature dependence of GSA. This result suggests that the trend in γ measured between 10 °C and 90 °C could be extrapolated to temperatures beyond this range with reasonable accuracy, where the temperature dependence of the pump GSA has been measured [18].

Further study would be required to determine the impact of temperature on pump ESA at other pump wavelengths, but for red diode pumping these results highlight another benefit to efficiency through moving towards higher temperatures in Alexandrite.

4. Modelling Alexandrite

4.1. Theoretical model

The energy level system considered in Fig. 7 was solved for end-pumping in our previous work [17]. The key results for pump threshold and slope efficiency of the laser cavity analysis are summarised here for reference. The integrated inversion $F = \int_0^l n_1(z)\mathrm{d}z/N$ defines the properties of the laser cavity, where z is the coodinate along the gain medium with $z = 0$ the incident plane

Optics EXPRESS

for end pumping, l is the length of the gain medium, and N is the total active lasing species concentration. During lasing its value is determined by the laser round trip gain condition giving

$$F = \frac{-\ln[(1-L)R] + 2\alpha_a l}{2(\alpha_e + \alpha_a - \alpha_{1a})}, \tag{3}$$

where L is the round trip fractional cavity loss, R is the output coupler reflectance, and $\alpha_i = \sigma_i N$ for any label i.

Upon solving the rate equations of the system, the associated laser threshold incident pump intensity, $I_{0\text{th}}$, is

$$\frac{I_{0\text{th}}}{I_s} = \frac{1}{\gamma\eta_{p,0}}\left(\frac{e^{\alpha_1 F} - 1}{1 - Te^{\alpha_1 F}}\right), \tag{4}$$

where $I_s = h\nu_p/(\sigma_0\tau_f)$ is the pump saturation intensity, h is the Planck constant, ν_p is the pump radiation frequency, $\gamma = \sigma_1/\sigma_0$ is the ratio of pump ESA to GSA and quantifies the pump ESA strength, $T = e^{-\alpha_0 l}e^{-(1-\gamma)F}$ is the saturated pump transmission through the gain medium, and $\eta_{p,0}$ is the fraction of ions transferred from the upper pump level n_2 to the upper laser level n_1 - this could be less than 100% if there is decay from n_2 into a non-lasing band.

The laser was shown to have a non-linear output versus pump input power with potentially bistable operation [17]; however, for the experimental system considered the output power was approximately linear with input pump power and its asymptotic limiting slope efficiency η_s can be used

$$\eta_s = \eta_{oc}\eta_q\eta_a\eta_p, \tag{5}$$

where η_{oc} is the output coupling efficiency, η_q is the Stokes efficiency, η_a is the pump absorption fraction, and $\eta_p = \eta_{p,0}\eta_{p,ESA}$ is the overall pump quantum efficiency including the effect of ESA in $\eta_{p,ESA}$. This is the fraction of absorbed pump photons that generate population inversion. This is the common form of the slope efficiency, with the constituent terms given by

$$\eta_{oc} = (1-\gamma_l)\left[\frac{-\ln R}{-\ln R - \ln(1-L) + 2\gamma_l\alpha_a l}\right], \tag{6}$$

$$\eta_q = \lambda_p/\lambda_l, \tag{7}$$

$$\eta_a = 1 - T, \tag{8}$$

$$\eta_{p,ESA} = \frac{\alpha_1}{(1+a\gamma)}\left[\frac{1 - Te^{\alpha_1[F-a(l-F)]}}{1-T}\right]\left[\frac{F - a(l-F)}{e^{\alpha_1[F-a(l-F)]} - 1}\right]. \tag{9}$$

where $\gamma_l = \sigma_{1a}/(\sigma_e + \sigma_a)$ quantifies the laser ESA fraction, $\gamma = \sigma_1/\sigma_0$ quantifies the pump ESA fraction, $a = \sigma_a/\sigma_e$, λ_p and λ_l are the pump and laser radiation wavelengths respectively.

The intrinsic slope efficiency η_0 is the maximum possible slope efficiency of a gain medium. It is found from Eq. (5) by eliminating cavity dependent terms (R, L, l), giving

$$\eta_0 = \eta_{p,0}\frac{\lambda_p}{\lambda_l}\left[\frac{1-\gamma_l}{1 + (\sigma_a/\sigma_e)\gamma}\right]. \tag{10}$$

The Stokes efficiency (λ_p/λ_l) is easily identified in the expression. The effect of laser ESA is apparent in the γ_l term coming from the output coupling efficiency η_{oc}. Pump ESA is included with the γ term, from the pump quantum efficiency η_p, and is coupled to laser GSA. In an ideal cavity with no loss, laser GSA requires population inversion at threshold for net gain, as shown in Eq. (3), resulting in an intrinsic pump ESA loss. In a three, four or quasi-three level system the intrinsic efficiency is just the product of the Stokes efficiency and $\eta_{p,0}$; however, both laser and pump ESA result in unavoidable losses when present, as given by the term in square brackets in Eq. (10).

Optics EXPRESS

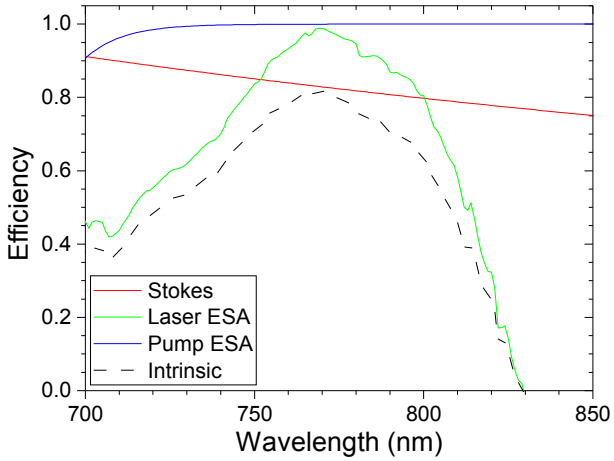


Fig. 11. The wavelength dependence of the instrinic slope efficiency $\eta_0(\lambda_l)$ of Alexandrite at 28 °C for red diode pumped at 636 nm, with the constituent terms of the Stokes, laser ESA and pump ESA efficiencies.

4.2. *Efficiency limits of Alexandrite*

The intrinsic slope efficiency η_0 is a useful guide to the ultimate performance of a gain medium that can be expected, and it is shown for Alexandrite as a function of wavelength in Fig. 11 along with its constituent components for red diode pumping at 636 nm and 28 °C crystal temperature. In Alexandrite, $\eta_{p,0} = 1$ because all absorbed pump photons from GSA decay into the upper laser level [1]. The peak intrinsic efficiency of 82 % is at 770 nm, where the limiting factor is the Stokes efficiency. An efficiency of near or greater than 40 % is available from 700 nm to 815 nm, illustrating the suitability of Alexandrite as a tunable source. It is possible to achieve efficiencies close to the intrinsic efficiency in Alexandrite. Using a red dye laser pump source at 645 nm, a 64 % slope efficiency at 753 nm laser wavelength has been demonstrated [22].

A main factor in the intrinsic efficiency comes from laser ESA, however its effect is minimised at 770 nm where there is negligible laser ESA [15, 23]. At either side of this peak the efficiency decreases due to the increasing laser ESA cross section, but occurs at a higher rate towards longer wavelengths where the emission cross section is decreasing. There is an intersection point between the emission and ESA cross sections at 830 nm. At this point no gain is possible and the efficiency becomes zero.

The intrinsic slope efficiency is a function of temperature due to the temperature dependence of all cross sections in Alexandrite. The dominant effect is from laser ESA in the output coupling efficiency, which is shown against laser wavelength at different crystal temperatures in Fig. 12. There is a shift in the intersection point of the laser emission and ESA cross sections that increases the long wavelength lasing limit, which is in agreement with previous experimental demonstrations [2]. It is difficult to minimise the effect of laser ESA as it is isolated in the efficiency terms and only a factor of material properties.

In the intrinsic slope efficiency, the pump ESA component is only significant below 720 nm where laser GSA is largest; however, in a real laser non-zero cavity losses means the pump ESA needs to be more carefully considered. The pump quantum efficiency is shown in Fig. 13 as a function of wavelength with nominal laser cavity parameters of $R = 0.98$ and $L = 0.01$ to illustrate its behaviour in a realistic laser at different temperatures. As $\eta_{p,0} = 1$ in Alexandrite only pump ESA contributes to the pump quantum efficiency and $\eta_p = \eta_{p,ESA}$.

To understand the form of the pump quantum efficiency across the tuning range it is important

Optics EXPRESS

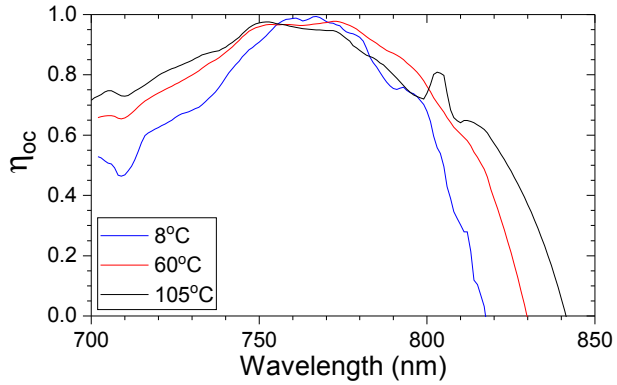


Fig. 12. The maximum output coupling efficiency $(1-\gamma_1)$ versus laser wavelength at different crystal temperatures.

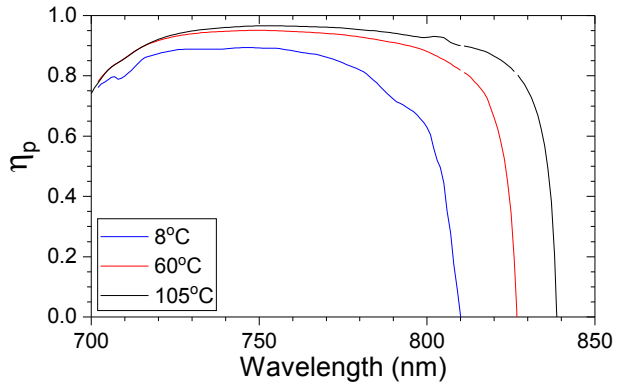


Fig. 13. The pump ESA quantum efficiency versus laser wavelength for different crystal temperatures. In Alexandrite $\eta_p = \eta_{p,ESA}$.

to note that the pump ESA quantum efficiency decreases for increasing integrated population inversion F, Eq. (9). Where there is a higher net gain coefficient $(\sigma_e - \sigma_{1a})$ there will be a lower threshold inversion and a correspondingly higher pump quantum efficiency. The efficiency is maximised in the region near 750 nm, the peak net gain in Alexandrite. Towards shorter and longer wavelengths the net gain decreases giving a lower efficiency, but decreases at a much greater rate towards long wavelengths where the net gain reduces to zero. This point of zero net gain occurs at longer laser wavelengths for increasing crystal temperatures, as clearly seen in Fig. 13.

The effect of pump ESA is less constraining than that of laser ESA because it depends on the inversion level, which can be controlled to some extent by the cavity design parameters of L and R.

4.3. Analysing cw lasing

With an understanding of the underlying processes in Alexandrite lasing, the combination of them in a cw laser can be analysed. The medium was modelled using the pump ESA ratio measured in Fig. 10 and all other parameters were taken from the literature. The cavity parameters were $R = 98\,\%$, $L = 0.5\,\%$, $l = 4\,\text{mm}$, and a circular pumped area diameter of 180 µm, similar to the experimental cavity in Section 2. The threshold and slope efficiency against laser wavelength and

Optics EXPRESS

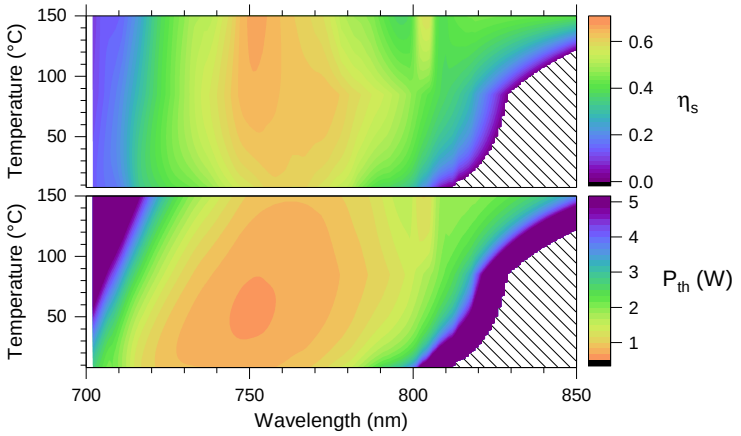


Fig. 14. From the model in Eqs. (4)-(9), the slope efficiency (top, η_s) and threshold (bottom, P_{th}) of an Alexandrite laser with output coupler $R = 98\,\%$ and round trip loss $L = 0.5\,\%$, versus laser wavelength and crystal temperature. The hatched regions are where lasing is not possible due to zero net gain.

crystal temperature are shown in Fig. 14 for this system.

Between 750 nm to 770 nm temperature has the least effect on both the threshold and slope efficiency, which is the region of 4-level lasing where the effects of laser GSA, pump and laser ESA are minimised. The product of the fluorescence lifetime and the emission cross section is the dominant temperature dependent factor in the laser threshold, via I_s in Eq. (4), but as this product is approximately constant with temperature, see Fig. 9, so is the threshold.

Below 750 nm laser GSA becomes increasingly significant, with both shorter wavelengths and higher crystal temperatures increasing the laser GSA, which is the limiting factor for short wavelength lasing. A higher GSA requires more inversion for gain and increases the threshold. This means that colder crystal temperatures are optimum for short wavelength lasing. Shorter crystals are also preferential for short wavelength operation because unpumped population will increase the laser threshold, see the $2\alpha_a l$ loss term in Eq. (3). There is a negligible impact of temperature on the slope efficiency, mainly due to the pump quantum efficiency being typically invariant with temperature in this region, see Fig. 13.

Above 770 nm laser GSA no longer has any effect and laser ESA is the cause of the temperature and wavelength dependent behaviour. As described in Section 4.2, laser ESA creates a point of zero net gain at increasingly longer wavelengths for higher crystal temperatures. Higher temperatures are favoured in this wavelength region to maximise the available gain. This both reduces the threshold and makes certain wavelengths accessible by moving the point of zero net gain. The efficiency increases with temperature because the laser ESA efficiency increases (Fig. 12) along with the pump quantum efficiency significantly improving (Fig. 13). This is due to the higher emission cross section, hence a larger gain, that reduces the threshold population inversion. This behaviour will be common to all Alexandrite lasers due to the intrinsic nature of the laser ESA to Alexandrite.

5. Conclusion

This work has presented experimental results from two diode end-pumped Alexandrite lasers. The first was a low loss compact cavity, which achieved a record slope efficiency of 54% with respect to absorbed pump power with an output power of 1.2 W. The second was a wavelength tunable laser using an intracavity birefringent filter. The vibronic tuning range was 714 nm to

Optics EXPRESS

818 nm, which is a record lowest wavelength and broadest tuning range for a diode pumped Alexandrite laser. An important factor in this result was optimising the crystal temperature throughout the tuning range, which could be further improved using a crystal oven capable of a larger temperature range.

Through an analytical model, an Alexandrite laser was simulated across its laser tuning range and from 8 °C to 150 °C crystal temperature, which elucidated features of the experimental lasers. It was shown that low temperatures are beneficial for short wavelength lasing due to reduced laser GSA and lower laser threshold. High temperatures are required for lasing at longer wavelengths, improving laser thresholds and efficiencies through both laser and pump ESA effects, in addition to extending the possible long wavelength lasing limit. Also, the lowest threshold laser wavelength does not have the highest slope efficiency.

The pump ESA cross section ratio $\gamma = \sigma_1/\sigma_0$ was measured for the first time with varying crystal temperature and found to decrease approximately linearly from 0.8 at 10 °C to 0.7 at 90 °C. This completes the temperature dependent model of Alexandrite, with parameters required by the analytical model now available with temperature dependence in this result and the literature.

This work demonstrates the importance of crystal temperature for Alexandrite laser design, with modelling shown to be an accurate predictor of performance. Pulsed Alexandrite systems are also of interest with applications including remote sensing. These will exhibit temperature dependent effects, similarly to the cw case presented, but with potentially considerable differences due to the impact of the temperature dependent fluorescence lifetime and the higher stored inversion under Q-switched conditions. This regime would be worthy of further analytical and experimental study.

Funding

Imperial College London

Acknowledgements

WKJ is supported by an Imperial College President's PhD Scholarship

155.198.12.188 {ts '2018-03-20 05:12:59'}